Nat Hazards (2011) 59:665–680
DOI 10.1007/s11069-011-9788-6

ORIGINAL PAPER

The importance of digital elevation model resolution on granular flow simulations: a test case for Colima volcano using TITAN2D computational routine

L. Capra · V. C. Manea · M. Manea · G. Norini

Received: 1 September 2010 / Accepted: 27 December 2010 / Published online: 30 March 2011

Abstract The mobility of gravity-driven granular flows such as debris flows or pyroclastic density currents are extremely sensitive to topographic changes, such as break in slopes, obstacles, or ravine deviations. In hazard assessment, computer codes can reproduce past events and evaluate hazard zonation based on inundation limits of simulated flows over a natural terrain. Digital Elevation Model (DEM) is a common input for the simulation algorithm and its accuracy to reproduce past flows is crucial. In this work, we use TITAN2D code to reproduce past block-and-ash flows at Colima volcano (Mexico) over DEMs with different cell size (5, 10, 30, 50, and 90 m) in order to illustrate the influences of the resolution on the numeric simulations. Our results show that topographic resolution significantly affects the flow path and runout. Also, we found that simulations of past flows with the same input parameters (such as the basal friction angle) over topography with different resolutions resulted in different flow paths, areas, and thickness of the simulated flows. In particular, the simulations performed with the 5- and 10-m DEMs produced similar results. Also, we obtained consistent simulation results for the 30- and 50-m DEMs. However, for the coarser 90-m DEM results are largely different and inaccurate. We recommend generating a benchmark table in order to acquire characteristic values for the basal friction angle of studied events. In case of rugged topographies, a DEM with high resolution should be used for more confident results.

Keywords Pyroclastic flow · Granular flow simulation · Volcanic hazard · TITAN2D

1 Introduction

Gravity-driven granular flows, such as debris flows or pyroclastic density currents, are extremely sensitive to topographic changes during transport (Fisher 1990, 1995; Branney

L. Capra (✉) · V. C. Manea · M. Manea · G. Norini
Computational Geodynamics Laboratory, Centro de Geociencias, Campus Juriquilla, Queretaro, Universidad Nacional Autónoma de México, México City, México
e-mail: lcapra@geociencias.unam.mx

and Kokelaar 2002; Sulpizio and Dellino 2008). Break in slopes, obstacles, and ravine deviations are among the main factors in changing flow trajectories and run-out distances. In hazard assessment, computer routines can successfully reproduce past events and provide a hazard zonation based on inundation limits of simulated flows over a natural terrain. At present, several computational routines (i.e., TITAN2D, LAHARZ, FLOW3D) (Kover 1995; Schilling 1998; Patra et al. 2005) are currently used to simulate gravity-driven flows over topographies obtained from stereo coverage of satellite imagery (e.g. ASTER—Advanced Spaceborne Thermal Emission and Reflection Radiometer), radar data (e.g. SRTM—Shuttle Radar Topography mapping Mission), laser altimetry (e.g. LIDAR—Light Detection and Ranging), and generic vector data (e.g., contour lines from topographic maps). Despite the variability of the input parameters required by each routine in order to perform a numeric simulation, a Digital Elevation Model (DEM) is a common input for simulation algorithms. Previous works already evidenced the importance of DEM spatial resolution on the accuracy of numeric simulations, for example, for the LAHARZ routine used to delineate lahar hazard inundation zones (Stevens et al. 2002; Hubbard et al. 2007; Davila et al. 2007).

The aim of our work is to quantify how DEM resolution and accuracy affect the simulation results. For this purpose, we use TITAN2D, a modeling algorithm developed by Patra et al. (2005) for simulating granular flows. In particular, we use TITAN2D to reproduce past block-and-ash flows (BAFs) at Colima volcano in Mexico. The Colima volcano is a prominent volcanic edifice with an altitude of 4,260 m a.s.l., located 100 km south from Guadalajara city and 30 km north from Colima city (Fig. 1). It is one of the most active volcanoes in the world nowadays, presenting Merapi and Soufriere dome type collapses, Vulcanian and Plinian explosive eruptions, and extrusions of lava flows and domes (Macias et al. 2006; Saucedo et al. 2005; Luhr et al. 2010).

TITAN2D routine has already been extensively applied to evaluated small-scale pyroclastic flows, BAFs and rock avalanches for several volcanoes, such as the Popocatépetl, Nevado de Toluca, Chichón and Colima in Mexico (Pitman et al. 2003; Bursik et al. 2005; Rupp et al. 2006; Capra et al. 2008; Macias et al. 2008; Murcia et al. 2010; Sulpizio et al. 2010), Merapi volcano in Indonesia (Charbonnier and Gertisser 2009), Mt. Taranaki, New Zealand (Procter et al. 2010), Little Tahoma Peak in the USA (Stinton et al. 2004; Sheridan et al. 2005), and Mount Etna in Italy (Norini et al. 2008). The outcomes of these studies have highlighted the uncertainties in objectively defining input parameters for realistic simulations of volcaniclastic flows. These studies focus mostly on the incertitude of those parameters that govern flow mobility, such as internal and basal friction angle (i.e., Charbonnier and Gertisser 2009; Procter et al. 2010). Recently, Sulpizio et al. (2010) have introduced constrains on the effect of DEM resolution over the basal friction angle (ϕ_b), one of the main parameters that determine the flow runout. The ϕ_b corresponds to the minimum slope over which a granular material starts to move from its static position. The generic approach is to simulate past flows using a range of basal friction angles which depends on the DEM resolution. In fact, for low-resolution DEMs, the slope is smoothed and granular flows travel farther downstream even for low basal friction angles. In this work, we study in a systematic way how different DEM resolutions influence the output of simulations reproducing past pyroclastic flows, especially where topography is characterized by sudden changes in slope or close curves in deep ravines. We also investigate the range of different basal friction angles that accurately reproduce the same flow event over DEMs with different resolutions.

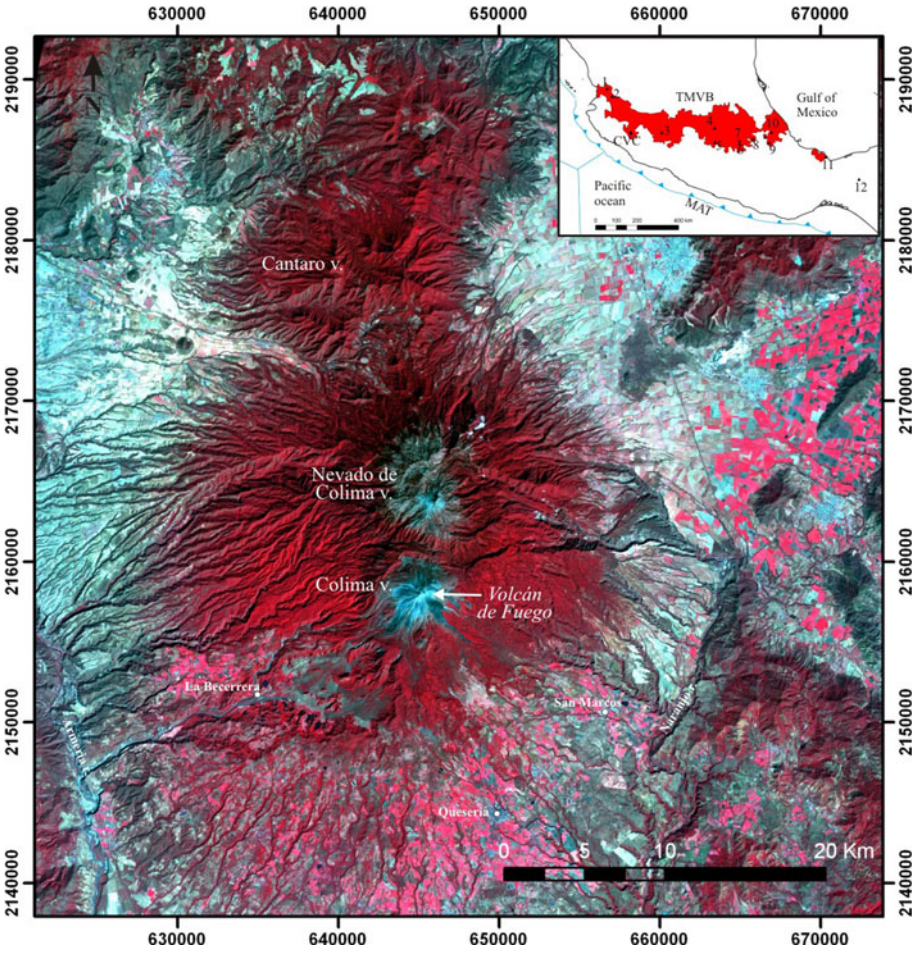

Fig. 1 ASTER image showing the Colima volcano and surrounding area. The *inset* shows a sketch map of the Trans-Mexican Volcanic Belt with the location of the CVC and other active volcanoes: *1* San Juan; *2* Ceboruco; *3* Tancitaro; *4* Jocotitlán; *5* Nevado de Toluca; *6* Popocatépetl; *7* Ixtaccíhuatl; *8* La Malinche; *9* Pico de Orizaba; *10* Cofre de Perote; *11* San Martín; *12* El Chichón

2 Methodology

2.1 TITAN2D

TITAN2D code was originally designed to simulate dry granular flows from an initial source area of collapse over a natural terrain (Pitman et al. 2003; Patra et al. 2005), but it is also highly suited to simulating BAFs formed from the collapse of large portions of lava domes. The code is based on a model for an incompressible Coulomb flow adapted from the work of Savage and Hutter (1989) using a "shallow-water" depth-averaged approximation (Iverson and Denlinger 2001). Mass and momentum conservation equations are solved with a Coulomb friction term for the interface between the granular material and basal surface and also for the internal friction of the flowing media (Pitman et al. 2003).

The resulting hyperbolic system of equations is solved using a parallel adaptive mesh (Patra et al. 2005). In this study, we used the 2.0.1. release to perform all the parallel numeric simulations. Terrain data are entered into the algorithm via GRASS GIS (Geographic Resources Analysis Support System).

The main input parameters for running simulations areas follows: (1) the volume of the collapsed mass; (2) the basal friction angle (φ_b); and (3) the internal frictional angle (φ_i). The initial conditions required by TITAN2D are the following: the coordinates of the initiation point, the elongation and orientation of the collapsed mass, the initial velocity and direction, and the duration and mass flux rate of the initial pile of material (Sheridan et al. 2005; Charbonnier and Gertisser 2009; Procter et al. 2010). After the simulated flow starts, a criterion for determining its stop is crucial for an accurate assessment of the runout, since in numerical simulations a flow never stops if its basal friction angle is lower than the slope angle. This is an unrealistic condition for real flows, for which other physical parameters concur in flow stopping (e.g., aspect ratio of the sliding pile, kinetic and potential energy of the moving flow, shape of the valley, or channel for confined flows). Yu et al. (2009) proposed a stopping criterion for simulated flows to determine their maximum runout. For this global stopping criterion, a dimensionless average velocity is defined as:

$$V_2^* = \frac{V_{ave}\alpha^{0.5}}{\sqrt{gH_0 \tan \varphi_{bed}^{0.5}}} = 0.03 \quad (1)$$

where V_{ave} is the simulated average flow velocity, α is the transient aspect ratio of the sliding pile, g is the gravity acceleration, H_0 is the initial pile height, and φ_b is the basal friction angle (Yu et al. 2009). Based on this relation, it is possible to determine the minimum acceptable average flow velocity (V_{ave}) below which the flow stops. Yu et al. (2009) proposed an V_2* average value of 0.03 which represents the best fit of constant values of V_2* that a simulated flow reaches after a dimensionless time of $t^* = t/(2H_0/g)^{0.5}$. Sulpizio et al. (2010) have shown that the V_2* value is highly sensible to the φ_b value used to perform the simulation and actually dominates the other variables in Eq. (1) such as the V_{ave} and the H_0, suggesting to evaluate the average velocity for each individual simulation.

2.2 Digital elevation models

The DEMs we used for the simulations are obtained from a LiDAR coverage of the Colima volcano with a 5-m horizontal resolution (Davila et al. 2007). The original 5-m raster was resampled to obtain four new DEMs with coarser horizontal resolutions of 10, 30, 50, and 90 m, respectively, using a nearest neighbor algorithm. These DEMs were then exported in ASCI file format compatible with GRASS in order to obtain the file format required by TITAN2D. Coarser resolutions were chosen because they represent the most common available formats, such as the 30-m DEM from SRTM data for the USA (1 arc second) and 90-m (3 arc second) for the rest of the world, the 30-m DEM obtained from ASTER image, or the 50-m DEM used in Mexico interpolated from 1:50,000 scale topographic maps (with 10 or 20 m contour lines) by INEGI (Instituto Nacional de Estadistica, Geografía e Informática).

Figure 2 shows the main differences among several topographic profiles performed on a series of DEMs from LiDAR (5, 10, 30, 50, and 90 m) and from SRTM (90 m), ASTER (30 m), and INEGI (50 m) data. The SRTM 90-m DEM was obtained from the CGIAR Consortium for Spatial Information web portal (http://srtm.csi.cgiar.org/). The ASTER data were obtained from a 2007 ASTER image acquired from the USGS-EROS web site

(http://glovis.usgs.gov/). The ASTER 30-m DEM was extracted from the 1A 3 N and 3B VNIR bands using the SILCAST application (Sensor Information Laboratory Inc.).

Profiles from LiDAR DEMs (Fig. 2b–d) show that when the resolution decreases the topography is smoothed and the maximum elevation of obstacles and lateral terraces is reduced with a difference of up to 15 m in height. These variations in altitude have the potential to significantly modify the behavior of a simulated flow. In fact, depending on the topographic barrier heights, the flow could be able to overrun the obstacle or to turn around it. Comparing the LiDAR DEMs at 30-, 50-, and 90-m spatial resolution with the ASTER 30 m, INEGI 50 m, and SRTM 90 m, respectively, several significant differences can be easily identified (Fig. 2). Despite the evident difference in the volcano summit altitude (Fig. 2b, profile a-a'), the SRTM 90-m is similar to the LiDAR 90-m with a smoothed profile. However, the ASTER 30-m does not reproduce the complex topography visible in the LiDAR 30-m, and it is more similar to the SRTM 90-m DEM. The observed inaccuracy in altitude could be fixed if direct measurements are available, but the overall topography will maintain a low detail. Finally, the INEGI 50-m DEM has better altitude accuracy, and it is comparable with the LiDAR 50-m DEM.

2.3 High-performance computing cluster (HPCC)—HORUS

In 2008, our research group decided to take a challenge to the Computational Geodynamics Laboratory (CGL)—Geosciences Center at UNAM and start building a HPCC named Horus, where TITAN2D was compiled with MPICH v. 1.2.7. In its present configuration,

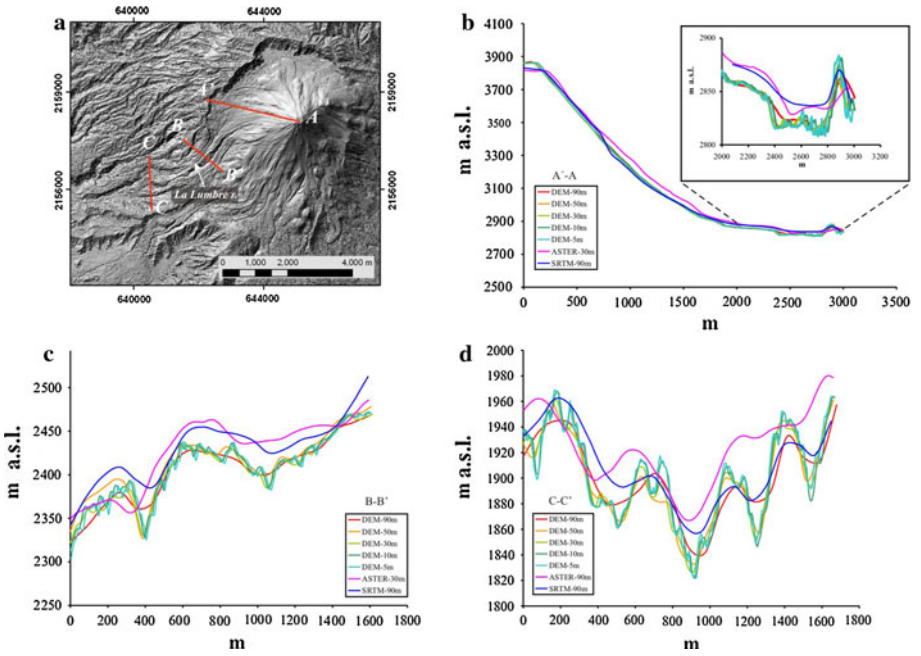

Fig. 2 **a** *Shadow* representation of the 5-m LiDAR DEM showing the location of topographic profiles obtained from the different DEMs resolutions as shown in figures **b**, **c**, and **d**. These profiles are evidencing the difference in accuracy in obstacle altitude and surface roughness, which represent one of the main factors in controlling flow simulations

Horus includes AMD Opteron (64 bit) 2.7 GHz dual- or quad-core processors and Intel 2.7 GHz (64 bit) quad-core processors. Horus has 43 compute nodes, each with 250 GB as local storage and 2 or 4 GB/core (Table 1).

In total, Horus contains 228 processing cores, 600 GB RAM memory, and a total of 30 TB for data storage. The cluster has a single 1000T centralized 48 ports switch that handles MPI traffic and is connected to a master node. We use as operating environment the open source Rocks Cluster Distribution-5.1

In order to test the performance of our HPCC against TITAN2D, several trials were ran with 2, 4, 8, 16, 32, 64 and 128 processors with fixed input parameters (Table 1) and a simulated time of 1,200 s. We also changed the number of computational cells from 5 to 10 and 15 for each DEM's resolution for a total of 105 runs. The number of cells is used by TITAN2D to determine the maximum permitted level of grid-cell refinement for the parallel adaptive mesh, which has direct implications on computational time and disk space storage.

2.4 Data representation

TITAN2D offers different output formats (tecplot/mshplot/GMFG Viz/Web Viz/Paraview or grass_sites). Here, we used the grass-sites format that can be easily imported into ARCGIS@ after the application of a simple script that automates the post-processing of all files generated during the numeric simulations performed on Horus (Appendix). The post-processed files contain for each site the latitude, longitude, flow thickness, and velocity, among others parameters. For each simulated step, where the time interval is set at the beginning of the simulation, TITAN2D produces a file in the grass-sites format. Therefore, it is possible to represent a single step of a simulation after a determined time interval, or the entire flow path using all steps. The methodology employed to visualize the entire flow path is to merge in ARCGIS (ESRI) all steps in a single file and then performing a point

Table 1 Hardware configuration of Horus

Computing nodes (34 servers)	
No. of processors	One or two per computing node
Type of processors	AMD Opteron and Intel (64 bit, dual- and quad-core)
Clock speed	2.6 GHz or higher
Local memory	2 or 4 GB/core
Local storage	250 GB—SATA
Network	1000T Ethernet
Master node (login node)	
No. of processors	Two (1 server)
Type of processors	AMD Opteron (64 bit, dual-core)
Clock speed	2.8 GHz
Local memory	2 GB/core
Local storage	2 × 1 TB SATA
Network	1000T Ethernet (two ports)
RAID	RAID 5 card (256 MB)
Network (1 switch)	
Network	1000T-48 ports unmanaged high performance switch
Storage (2 DAS)	
Storage	30 TB RAID 5 of direct attached storage

Table 2 Input parameters used to perform simulations

Pile starting point			Pile dimension (m)		
UTM E	UTM N		H	R_1	R_2
644879.58	2158137.69		45	75	75
DEM resolution (m)	5	10	30	50	90
No. of cells	5	10	20		
ϕ_b	30°				
ϕ_i used for benchmark	5°	10°	15°	20°	25°
ϕ_i used for the 2004 BAF	11°				

Parameters used as input for TITAN2D simulations. See text for more explanations

H pile height, R_1 mayor pile radius, R_2 minor pile radius, ϕ_b basal friction angle, ϕ_i internal friction angle

statistic analysis (maximum flow thickness around each point over a specified neighborhood) to obtain the maximum flow depth for each point around a minimum square area.

2.5 Input data

To determine how DEM resolution affects the basal friction angle, several trials were performed with basal friction angles ranging from 5° to 25° at a 5° interval. The other input parameters, such as the pile dimension, starting point, and the internal friction angle, were considered fixed for all the simulations (Table 2). In particular, the internal friction angle was set at 30°, a common value used in previous works (i.e. Sheridan et al. 2005; Rupp et al. 2006; Capra et al. 2008). The input volume and starting point correspond to the 2004 BAF at La Lumbre ravine, already simulated by Sulpizio et al. (2010). This pyroclastic flow is particularly suitable for our benchmark, because it is characterized by several important changes in curvature of ravines and breaks in slope (Fig. 2a). These morphological changes are useful to better quantify the importance of DEM resolution to simulate past events and to assess the hazard posed by volcanic granular flows.

3 Results

3.1 Computational efficiency

In Fig. 3, the relation between the number of cores and the duration of simulation after 1,200 s of flow is shown. Our computational system has the best performance using 16–32 processors, while using 2 or 128 processors the simulation takes almost the same time or even longer for 128 processors. This is caused probably by heavy data traffic between computing nodes. At 5-cells refinement (Fig. 3a), simulations have a longer duration as DEM resolution increases, but at 20-cells duration is fairly similar independently of the DEM resolution (Fig. 3c).

3.2 Stopping velocity

Stopping velocity is an important element recently introduced by Yu et al. (2009) and is used as a criterion to define at which point of the simulation the flow stops. As already

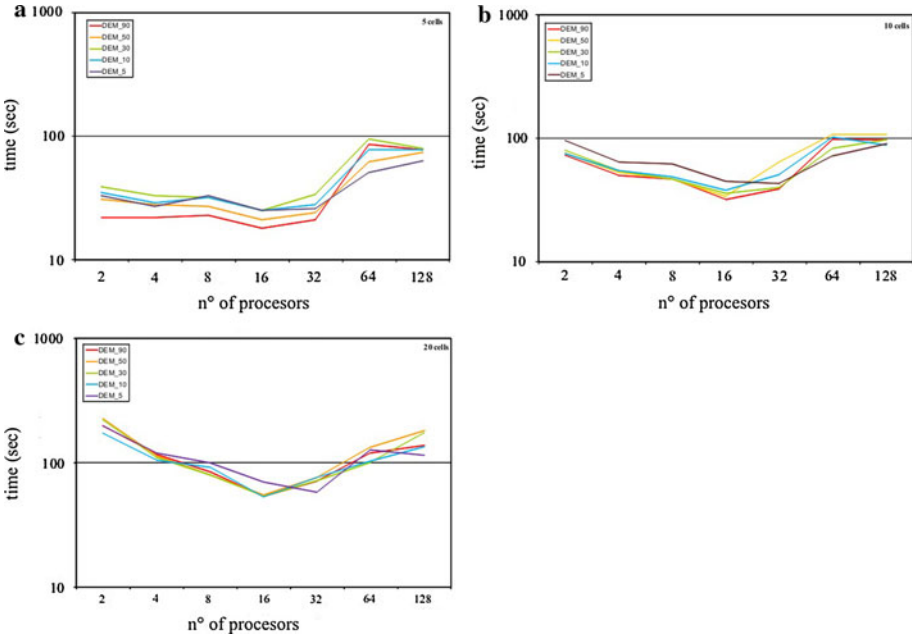

Fig. 3 Diagrams showing the simulated time for different DEMs resolutions as a function of processing cores, and for different cell numbers at **a** 5, **b** 10, and **c** 20. The *vertical axis* is wall time (s), the real time spent by the simulation on Horus

mentioned, the adimensional average velocity (V_2*) mostly depends on the initial pile dimension, the transient pile aspect, and the internal friction angle. Yu et al. (2009) proposed an average value of 0.03 for V_2* in confined and unconfined flows. In our work, several trials were performed to illustrate how V_2* changes with both, the basal friction angle and DEM resolution. In particular, the DEM resolution modifies the width and depth of the ravines (Fig. 3), with direct consequence on the transient pile aspect (α) and consequently on the V_2* value. Figure 4 shows the results obtained by maintaining fixed the DEM resolution while changing the basal friction angle. In all DEMs, at lower φ_b the V_2* increases with higher values for DEMs with enhanced resolution (Fig. 4). When comparing the V_2* value at fixed φ_b and different DEM resolutions, we encountered a similar pattern (Fig. 5). In conclusion, lower DEM resolutions determine higher V_2* values, being more evident as φ_b decreases.

3.3 Basal friction angle versus DEM resolution

To better understand the effect of the DEM resolution on the inundation limits of simulated flows, the same input parameters *(i.e.* φ_b of 13°) are used (Table 2). Figure 6 shows the visualization for the first 60 s of the flow and at its final depositional steps (calculated with the V_2* stopping velocity criterion). Our results show that as DEM resolution decreases, the flow reaches longer runout. Only with the fine resolution DEMs of 5 and 10 m (Fig. 6b, c), the flow is confined by the caldera rim and enters into the main ravine. For the other coarser DEMs, the flow overruns the topographic barrier and spreads over the flank of the volcano. Figure 7a shows the trajectory of the simulated flows through their central flow path. Whereas for the 5- and 10-m DEMs the trajectory is deviated by the caldera rim, for

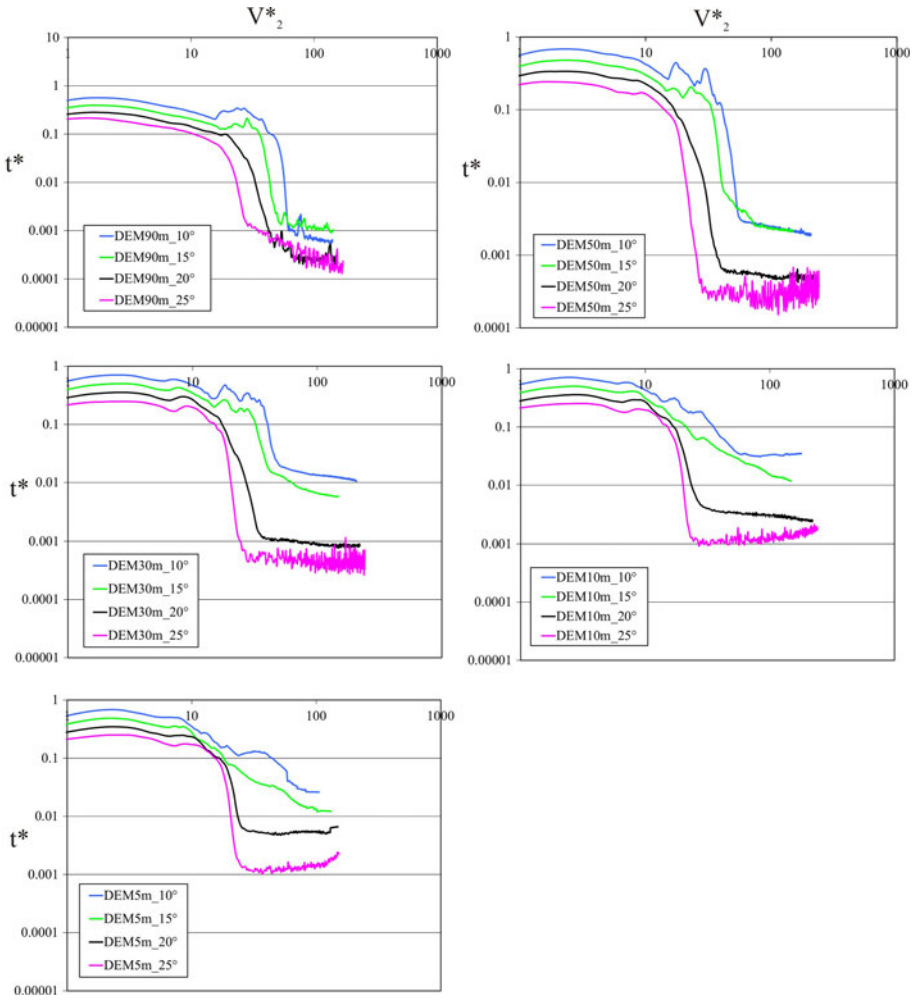

Fig. 4 Diagrams showing the variation of the stopping velocity V^*_2 versus the dimensionless time t^* at a fixed DEM resolution and varying the basal friction angle. The DEM#_#° abbreviation in legend (i.e., DEM90_1°0) stands for *D*# DEM resolution and *A*# value of the basal friction angle

the other cases, the flow path reassembles a fairly rectilinear path. It is also worth observing the behavior of the maximum average velocity of simulated flows (Fig. 7b). For the 5- and 10-m DEMs, where the flow is confined by the caldera rim, the flow gradually decelerates after the average velocity reaches its maximum. In contrast, for coarser DEMs resolution, the flow decelerates when it overruns the caldera rim and then reaccelerate to reach a second peak of the maximum average velocity (Fig. 7b). To better demonstrate this effect, the 2004 BAF emplaced in the La Lumbre ravine is here reproduced over the 5-m DEM. The input parameters are chosen as those used by Sulpizio et al. (2010) to reproduce the runout of this pyroclastic flow (Fig. 8a; Table 2). Then, the same simulation is run over the other DEMs. After 60 s, the simulated flow reveals that only with the 5-m DEM the flow keeps confined into the La Lumbre ravine (Fig. 8a). In the other cases (Fig. 8b–d), using a φ_b of 11° is inappropriate, since the flow overflows the caldera rim and

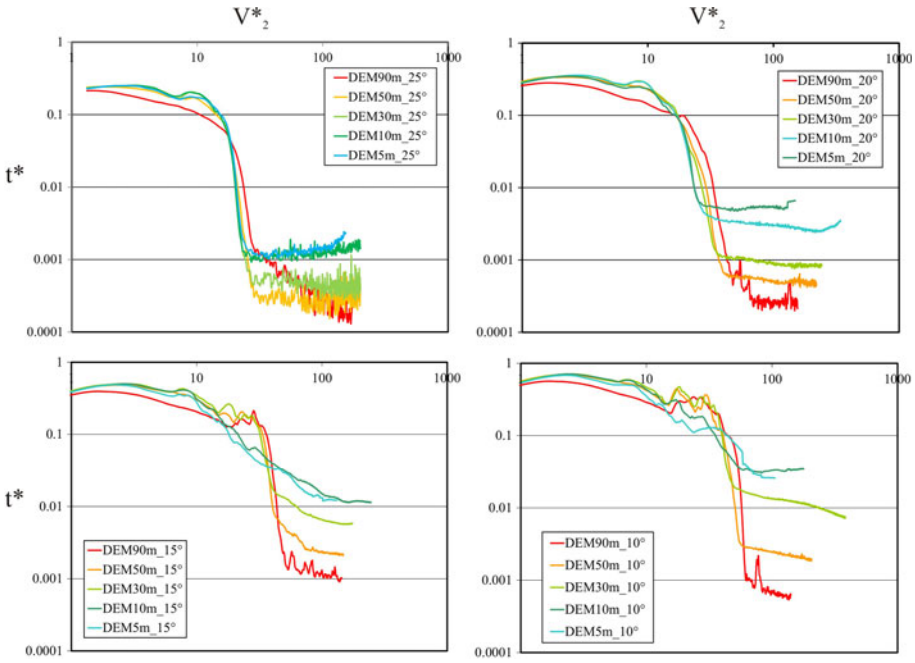

Fig. 5 Diagrams comparing the stopping velocity V^*_2 versus the dimensionless time t^* at a fixed basal friction angle and varying the DEM resolution. The DEM#_#° abbreviation in legend (i.e., DEM90_10°) stands for *DEM*# DEM resolution and #° value of the basal friction angle

subsequently subdivides into more ravines reaching greater runout and lower thickness. With the 90-m DEM, it is impossible to run the same simulation, since the φ_b of 11° is to low and the pile completely spread on the topography. To reproduce the 2004 flow on DEMs with lower resolution, it is necessary to use a greater φ_b value. For example, for the 50-m DEM a φ_b of 16° was suitable in order to obtain comparable results with the 5-m DEM simulation (Fig. 8e, f) but only for the runout. However, the thickness of the simulated flow does not reproduce the observed 3-m-thick front of the deposit, which is well reproduced only by the simulation with 5-m DEM (Fig. 8c).

4 Discussion

Numerous GIS-enabled software packages (TITAN2D, Patra et al. 2005; FLOW3D, Malin and Sheridan 1982; Kover and Sheridan 1993; and LAHARZ, Schilling 1998) have been developed for either predicting the path and extent of volcanic flows or visualizing their effects and potential impacts to civil infrastructures. It has been already demonstrated that LAHARZ, a routine to determine lahar inundation zones, is largely sensitive to the spatial resolution of the digital elevation data (i.e., Stevens et al. 2002; Davila et al. 2007; Hubbard et al. 2007). High-resolution DEMs can keep confined lahars using small flow volumes. On the other hand, for low-resolution DEMs larger volumes are needed to reach the same runout. Our modeling results show that the DEM resolution is fundamental for BAF simulations with TITAN2D. Low-resolution DEMs, such as the 90-m DEM, are

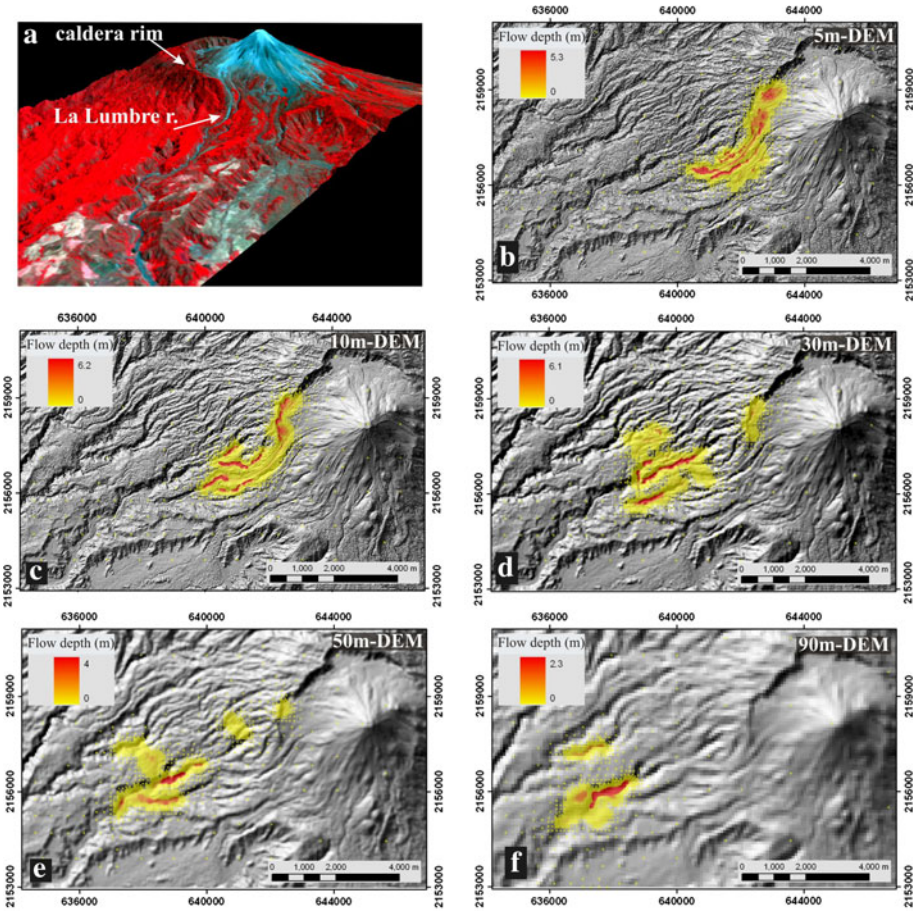

Fig. 6 **a** 3D view of the La Lumbre ravine. Note how the caldera rim acts as a topographic barrier to pyroclastic flows. From **b** to **f**: representation of the final depositional step (based on the V_2* value) for a simulated flow with a constant basal friction angle of 10° and for different DEM resolutions

inappropriate to reproduce BAF over irregular topographic path where obstacles and abrupt turns can suddenly diverge the simulated flow. Inaccuracy in both, altitude of topographic obstacles and depth of ravines, made impossible to reproduce past flows with similar φ_b for different DEM resolutions. The LiDAR data we used in this study are probably one of the best sources for topographic data, even better than SRTM or ASTER DEMs when resampled at the same resolution. The first main implication of this result resides in the impossibility to compare input data such as φ_b used to simulate BAF in different volcanoes or for the same event reproduced by other authors using different topographic data sources. In this sense, it is quite unrealistic to propose fixed φ_b values for some type of BAFs, since it will strongly depend on the DEM resolution. Our simulations performed with the 5- and 10-m DEMs are fairly similar, the same for the 30- and 50-m DEMs (Figs. 6, 8). However, for the 90-m DEM results are largely different and often inappropriate to accurately reproduce past flows. The same situation stands for the stopping velocity, since this parameter is largely dependent on the basal friction angles used to perform the simulations

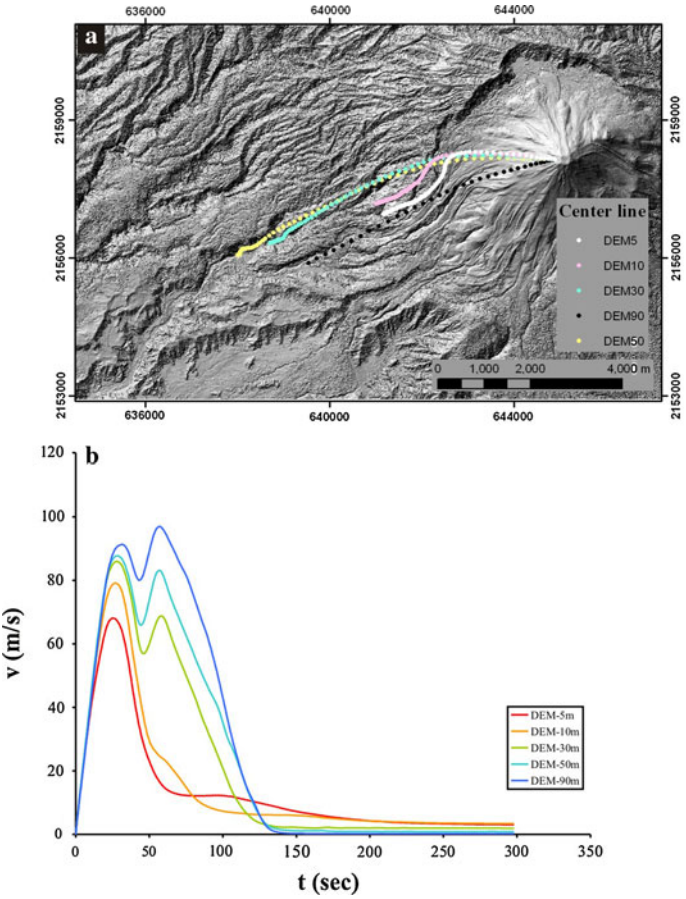

Fig. 7 **a** Trajectories for the *center lines* of flows simulated for different DEM resolutions, and **b** diagram showing the simulated average flow velocity (m/s) with time (*t*)

(Sulpizio et al. 2010). Even though DEM quality evaluation is not the main purpose of this work, the comparison of SRTM, ASTER, INEGI, and LiDAR data (Fig. 2) revealed that vector data obtained from topographic maps, as those available in Mexico, represent a good source to acquire a DEM with an appropriated resolution. It is worth noting that the free availability of SRTM data makes this source to be largely used in our scientific community. Even with a 90-m in spatial resolution, the SRTM DEM seems to be better than the DEM generated from ASTER images. However, the resolution of such DEM is probably too low to reproduce past flow over complicated topography such as the case for the 2004 La Lumbre BAF.

5 Conclusions

In this paper, we show that TITAN2D parallel code represents a useful tool to perform simulations of BAFs trajectory and maximum runout. As several works have already shown (i.e. Charbonnier and Gertisser 2009; Procter et al. 2010), the importance of input

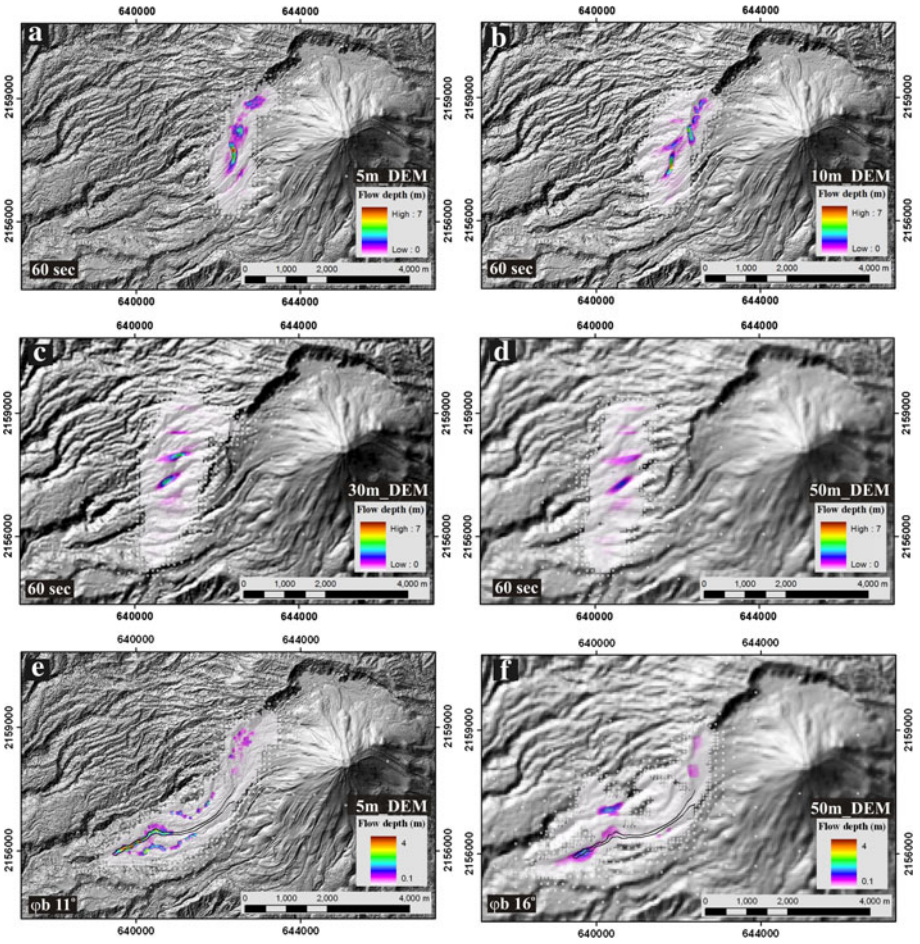

Fig. 8 Simulation results showing the trajectory and thickness of the 2004 pyroclastic flow emplaced in the La Lumbre ravine. **a**, **b**, **c**, and **d** modeling results of the flow after 60 s, over the 5, 10, 30, and 50 m DEM resolutions, respectively. **e** Numeric simulation that best fits the 2004 pyroclastic flow (*black line*, Sulpizio et al. 2010) with a basal friction angle of 11° for the 5-m DEM. **f**: numeric simulation that best fits the 2004 pyroclastic flow (*black line*, Sulpizio et al. 2010) using a basal friction angle of 16° and a 50-m DEM

parameters accuracy needed by this algorithm to reproduce past flows is crucial. Our work represents a significant contribution, evidencing that the source data, used to obtain the DEM over which the flow is simulated, represent a key input parameter that controls the simulation results. We strongly recommend determining the right set of input parameters by several trials in order to acquire characteristic values for the basal friction angle. In the particular case of rugged topography, a DEM with high resolution (i.e., 5–10 m) should be acquired in order to obtain confident simulation results.

Acknowledgments All numeric computations were performed at the Computational Geodynamics Laboratory—CGEO supercomputing facility (Horus). Financial support has been provided by PAPIIT (IN-106710) and CONACyT (99486) to Lucia Capra. We would like to thank Roberto Sulpizio and an anonymous reviewer for suggestions that improved this manuscript.

Appendix

```
#!/bin/bash
##################################
#This script permits modifying the file's structure (Changing delimiters from "|" and  "%" to "tab");
created June 2007 by Marina Manea & Vlad Manea, CGEO - UNAM
#Adapted by Lucia on 7th of August 2007, CGEO – UNAM
# This script can be optimized and adjusted for your needs
##################################
        # User input variables:
        ## Modify output file name as you wish
output_name="grass_p"
        # End of input variables
##################################
        ## OBS: You can choose how many steps you will need depending on your GRASS file
names. Most of these files come in order and are formed by a sequence of letters (in our case:
"grass_sites"), 8 numbers (if you have a file with "00000000" this is your first file), a "." followed by
"000". If you have only 9 files you can use only the first processing step. Otherwise, as the 8
numbers sequence start with "00000010" you might need to add the processing step no. 2. Just
modify the "echo" line for more on-screen control.
##################################
        ##print a message on screen showing the step no.
echo "Processing step 1/5..."

for ((COUNTER=0; COUNTER<10; COUNTER++)) ; do
        if [ -f grass_sites0000000$COUNTER.000 ]; then
        ##generate additional files
        ## change delimiters from "|" and  "%" to "tab"
cat  grass_sites0000000$COUNTER.000 |  awk '{values=$1; split(values,names,"|"); print
names[1],"\t",names[2],"\t",names[3],"\t",names[4],"\t",$2,"\t",$3,"\t",$4,"\t",$5}' >
test00000001$COUNTER.000
cat  test00000001$COUNTER.000 |  awk '{sub(/%/,"",$4); sub(/%/,"",$5); sub(/%/,"",$6);
sub(/%/,"",$7); sub(/%/,"",$8);print $1,"\t",$2,"\t",$3,"\t",$4,"\t",$5,"\t",$6,"\t",$7,"\t",$8}' >
test00000002$COUNTER.000
        ##generate final file in "txt" format, consisting of: output name (in our case: "grass_p", the
8 numbers (at this step: 7 "0" + the counter variable) and a "." followed by "txt"
cat header.txt test00000002$COUNTER.000 > $output_name"0000000"$COUNTER.txt
        ##remove additional files
rm test00000001$COUNTER.000
rm test00000002$COUNTER.000
        fi
done
##################################
##All the rest steps are variations of the first one and depend on your files number. In our case
we had to deal with file in which the variable COUNTER was < 100000.
echo "Processing step 2/5..."

for ((COUNTER=10; COUNTER<100; COUNTER++)) ; do
        if [ -f grass_sites000000$COUNTER.000 ]; then
                cat  grass_sites000000$COUNTER.000 |  awk '{values=$1;
split(values,names,"|"); print
names[1],"\t",names[2],"\t",names[3],"\t",names[4],"\t",$2,"\t",$3,"\t",$4,"\t",$5}' >
test0000001$COUNTER.000
                cat  test0000001$COUNTER.000 |  awk '{sub(/%/,"",$4); sub(/%/,"",$5);
sub(/%/,"",$6); sub(/%/,"",$7); sub(/%/,"",$8);print
$1,"\t",$2,"\t",$3,"\t",$4,"\t",$5,"\t",$6,"\t",$7,"\t",$8}' > test0000002$COUNTER.000
                cat header.txt test0000002$COUNTER.000 >
$output_name"000000"$COUNTER.txt
                rm test0000001$COUNTER.000
                rm test0000002$COUNTER.000
        fi
done
##################################
echo "Processing step 3/5..."

for ((COUNTER=100; COUNTER<1000; COUNTER++)) ; do
        if [ -f grass_sites00000$COUNTER.000 ]; then
```

```
                cat  grass_sites00000$COUNTER.000 |  awk '{values=$1;
split(values,names,"|"); print
names[1],"\t",names[2],"\t",names[3],"\t",names[4],"\t",$2,"\t",$3,"\t",$4,"\t",$5}' >
test000001$COUNTER.000
                cat  test000001$COUNTER.000 |  awk '{sub(/%/,"",$4); sub(/%/,"",$5);
sub(/%/,"",$6); sub(/%/,"",$7); sub(/%/,"",$8);print
$1,"\t",$2,"\t",$3,"\t",$4,"\t",$5,"\t",$6,"\t",$7,"\t",$8}' > test000002$COUNTER.000
                cat header.txt test000002$COUNTER.000 >
$output_name"00000"$COUNTER.txt
                rm test000001$COUNTER.000
                rm test000002$COUNTER.000
        fi
done
#################################
echo "Processing step 4/5..."

for ((COUNTER=1000; COUNTER<10000; COUNTER++)) ; do
        if [ -f grass_sites0000$COUNTER.000 ]; then
                cat  grass_sites0000$COUNTER.000 |  awk '{values=$1; split(values,names,"|");
print names[1],"\t",names[2],"\t",names[3],"\t",names[4],"\t",$2,"\t",$3,"\t",$4,"\t",$5}' >
test00001$COUNTER.000
                cat  test00001$COUNTER.000 |  awk '{sub(/%/,"",$4); sub(/%/,"",$5);
sub(/%/,"",$6); sub(/%/,"",$7); sub(/%/,"",$8);print
$1,"\t",$2,"\t",$3,"\t",$4,"\t",$5,"\t",$6,"\t",$7,"\t",$8}' > test00002$COUNTER.000
                cat header.txt test00002$COUNTER.000 > $output_name"0000"$COUNTER.txt
                rm test00001$COUNTER.000
                rm test00002$COUNTER.000
        fi
done
#################################
echo "Processing step 5/5..."

for ((COUNTER=10000; COUNTER<100000; COUNTER++)) ; do
        if [ -f grass_sites000$COUNTER.000 ]; then
                cat  grass_sites000$COUNTER.000 |  awk '{values=$1; split(values,names,"|");
print names[1],"\t",names[2],"\t",names[3],"\t",names[4],"\t",$2,"\t",$3,"\t",$4,"\t",$5}' >
test0001$COUNTER.000
                cat  test0001$COUNTER.000 |  awk '{sub(/%/,"",$4); sub(/%/,"",$5);
sub(/%/,"",$6); sub(/%/,"",$7); sub(/%/,"",$8);print
$1,"\t",$2,"\t",$3,"\t",$4,"\t",$5,"\t",$6,"\t",$7,"\t",$8}' > test0002$COUNTER.000
                cat header.txt test0002$COUNTER.000 > $output_name"000"$COUNTER.txt
                rm test0001$COUNTER.000
                rm test0002$COUNTER.000
        fi
done
#################################

echo "All DONE!"
```

References

Branney MJ, Kokelaar P (2002) Pyroclastic density currents and the sedimentaion of ignimbrites, vol 27. Geological Society Memoir, London, p 152

Bursik A, Patra A, Pitman EB, Nichita C, Macias JL, Saucedo R, Girina O (2005) Advances in studies of dense volcanic granular flows. Rep Prog PhyS 68:271–301

Capra L, Norini G, Groppelli G, Macías JL, Arce JL (2008) Volcanic hazard zonation of Nevado de Toluca Volcano. J Volcanol Geotherm Res 176:469–484

Charbonnier S, Gertisser R (2009) Numerical simulations of block-and-ash flows using the Titan2D flow model: examples from the 2006 eruption of Merapi Volcano, Java, Indonesia. Bull Volcanol 71:953–959

Davila N, Capra L, Gavilanes-Ruiz JC, Varley N, Norini G, Gomez-Vazquez A (2007) Recent lahars at Volcan de Colima (Mexico): drainage variation and spectral classification. J Volcanol Geotherm Res 165:127–141

Fisher RV (1990) Transport and deposition of a pyroclastic surge across an area of high relief: the 18 May 1980 eruption of Mount St. Helens, Washington. Geol Soc Am Bull 102:1038–1054

Fisher RV (1995) Decoupling of pyroclastic currents: hazard assessments. J Geophys Res 66:257–263
Hubbard B, Sheridan MF, Carrasco-Núñez G, Díaz-Castellón R, Rodríguez-Elizarrarás SR (2007) Comparative lahar hazard mapping at Volcan Citlaltépetl, Mexico using SRTM, ASTER and DTED-1 digital topographic data. J Volcanol Geotherm Res 160:99–124
Iverson RM, Denlinger RP (2001) Flow of variably fluidized granular masses across three dimensional terrain, I. Coulomb mixture theory. J Geophys Res 106:537–552
Kover TP (1995) Applications of a digital terrain model for the modeling of volcanic flows: a tool for volcanic hazard determination. Master Thesis, SUNY, Buffalo, p 62
Luhr J, Navarro-Ochoa C, Savov IP (2010) Tephrochronology, petrology and gepchemistry of Late-Holocene pyroclastic deposits from Volcán de Colima, México. J Volcanol Geotherm Res (in press)
Macias JL, Saucedo R, Gavilanes JC, Varley N, Velasco Garcia S, Bursik MI, Vargas Gutierres V, Cortes A (2006) Flujos piroclásticos asociados a la actividad explosiva del Volcán de Colima y perspectivas futuras. GEOS 25(3):340–351
Macias JL, Capra L, Arce JL, Espindola JM, Garcia-Palomo A, Sheridan MF (2008) Hazard map of El Chichón volcano, Chiapas, México: constraints posed by eruptive history and computer simulations. J Volcanol Geotherm Res 175:444–458
Malin MC, Sheridan MF (1982) Computer-assisted mapping of pyroclastic surges. Science 217:637–639
Murcia HF, Sheridan MF, Macías JL, Cortes GP (2010) TITAN2d simulation of pyroclastic flows at Cerro Machin Volcano, Colombia: hazard implications. S Am Earth Sci 29:161–170
Norini G, De Beni E, Andronico D, Polacci M, Burton M, Zucca F (2008) The 16 November 2006 flank collapse of the south-east crater at Mount Etna, Italy: study of the deposit and hazard assessment. J Gephys Res 114:B02204
Patra A, Bauer A, Nichita CC, Pitman EB, Sheridan MF, Bursik MI, Rupp B, Webber A, Stinton AJ, Namikawa L, Renschler C (2005) Parallel adaptive numerical simulation of dry avalanches over natural terrain. J Volcanol Geotherm Res 139:1–21
Pitman EB, Nichita CC, Patra A, Bauer A, Sheridan MF, Bursik MI (2003) Computing granular avalanches and landslides. Phys Fluids 15(12):3638–3646
Procter JN, Cronin SJ, Platz T, Patra A, Dalbey K, Sheridan MF, Neall V (2010) Mapping block-and-ash flow hazards based on Titan 2D simulations: a case study from Mt. Taranaki, NZ, Natural Hazards. doi: 10.1007/s11069-009-9440-x
Rupp B, Bursik M, Namikawa A, Patra A, Saucedo R, Macías JL (2006) Computational Modeling of the 1991 block and ash flow at Colima Volcano, Mexico. Geol Soc Am Special Paper 402:223–238
Saucedo R, Macias JL, Sheridan MF, Komorowski JC (2005) Modeling of pyroclastic flows of Colima Volcano, Mexico: implicatons for hazard assessment. J Volcanol Geotherm Res 139:103–115
Savage SB, Hutter K (1989) The motion of a finite mass of granular material down a rough incline. J Fluid Mech 199:177–215
Schilling S (1998) LAHARZ: GIS programs for automated mapping of lahar-inundation hazard zones. USGS open-file report, pp 98–638
Sheridan MF, Stinton AJ, Patra A, Pitman EB, Bauer A, Nichita CC (2005) Evaluating Titan2D mass-flow model using the 1963 Little Tahoma Peak avalanches, Mount Rainier, Washington. J Volcanol Geotherm Res 139:89–102
Stevens NF, Manville V, Heron DW (2002) The sensitivity of a volcanic flow model to digital elevation model accuracy: experiments with digitized map contours and interferometric SAR at Ruapehu and Taranaki volcanoes, New Zealand. J Volcanol Geotherm Res 119:89–105
Stinton AJ, Sheridan MF, Patra A, Dalbey K, Namikawa L (2004) Integrating variable bed friction into Titan2D mass-flow model: application to the Little Tahoma Peak avalanches, Washington. Acta Vulcanol 16:153–163
Sulpizio R, Dellino P (2008) Sedimentology, depositional mechanisms and pulsating behaviour of pyroclastic density currents. In: Gottsman J, Marti J (eds) Calderas volcanism: analysis, modeling and response. Elsevier, Amsterdam
Sulpizio R, Capra L, Sarocchi D, Saucedo R, Gavilanes-Ruiz JC, Varley N (2010) Predicting the block-and-ash flow inundation areas at Volcán de Colima (Colima, Mexico) based on the present day (February 2010) status. J Volcanol Geotherm Res 193:49–66
Yu B, Dalbey K, Webb A, Bursik M, Patra AE, Pitman B, Nichita CC (2009) Numerical issues in computing inundation areas over natural terrains using Savage-Hutter theory. Nat Hazards 50:249–267